chemengineering

MDPI

Article

Graphene-Wine Waste Derived Carbon Composites for Advanced Supercapacitors

Violeta Ureña-Torres [1], Gelines Moreno-Fernández [1,*], Juan Luis Gómez-Urbano [1,2], Miguel Granados-Moreno [1] and Daniel Carriazo [1,3,*]

[1] Centre for Cooperative Research on Alternative Energies (CIC energiGUNE), Basque Research and Technology Alliance (BRTA), Alava Technology Park, Albert Einstein 48, 01510 Vitoria-Gasteiz, Spain; violetauat@gmail.com (V.U.-T.); jlgomezurbano@cicenergigune.com (J.L.G.-U.); magranados@cicenergigune.com (M.G.-M.)

[2] Departamento de Química Orgánica e Inorgánica, Facultad de Ciencia y Tecnología, Universidad del País Vasco, UPV/EHU, 48080 Bilbao, Spain

[3] IKERBASQUE, Basque Foundation for Science, 48013 Bilbao, Spain

* Correspondence: mamoreno@cicenergigune.com (G.M.-F.); dcarriazo@cicenergigune.com (D.C.); Tel.: +34-945-297-108 (G.M.-F. & D.C.)

Abstract: In this work, we investigate the potential of a novel carbon composite as an electrode for high-voltage electrochemical double-layer capacitors. The carbon composite was prepared following a sustainable synthetic approach that first involved the pyrolysis and then the activation of a precursor formed by winery wastes and graphene oxide. The composite prepared in this way shows a very high specific surface area (2467 $m^2 \cdot g^{-1}$) and an optimum pore size distribution for their use in supercapacitor electrodes. Graphene-biowaste-derived carbon composites are tested as active electrode materials in two different non-aqueous electrolytes, the ammonium salt-based conventional organic electrolyte and one imidazolium-based ionic liquid (1 M Et_4NBF_4/ACN and EMINTFSI). It was found that the presence of graphene oxide led to significant morphological and textural changes, which result in high-energy and power densities of ~27 $W \cdot h \cdot kg^{-1}$ at 13,026 $W \cdot kg^{-1}$. Moreover, the devices assembled retain above 70% of the initial capacitance after 6000 cycles in the case of the organic electrolyte.

Keywords: biowastes; EDLC; 2-D carbons; advanced electrolytes

Citation: Ureña-Torres, V.; Moreno-Fernández, G.; Gómez-Urbano, J.L.; Granados-Moreno, M.; Carriazo, D. Graphene-Wine Waste Derived Carbon Composites for Advanced Supercapacitors. *ChemEngineering* **2022**, *6*, 49. https://doi.org/10.3390/chemengineering6040049

Academic Editor: Miguel A. Vicente

Received: 26 May 2022
Accepted: 24 June 2022
Published: 29 June 2022

1. Introduction

The rapid growth undergone by our society in the last decades has pushed us to look for new strategies in order to achieve sustainable development. This mainly involves the change of our current energy model based on the combustion of fossil fuels to a more eco-friendly one based on the use of renewable and greener sources, such as wind or solar energies. To attain this objective, it is necessary to develop new energy storage technologies that allow the use of these intermittent energies when they are not available [1]. Electrochemical capacitors, commonly known as supercapacitors, together with batteries, are the most widely used storage systems in portable devices, and their use is already beginning to be spread into larger applications such as electric vehicles or stationary energy storage stations [2]. Unlike batteries, where the charge is stored by faradaic processes, in supercapacitors, the charge is stored through an electrostatic process at the interface between the electrode and the electrolyte [3,4]. This mechanism does not involve ions insertion into the material's bulk; thus, its kinetics are not limited by diffusion processes, being able to provide higher power and a longer life-time than batteries [5]. These features make supercapacitors very attractive in a certain number of applications where reliability, wide operating temperature range, long-term stability or high power is required.

Electrical double-layer capacitors (EDLC) are typically formed by two similar electrodes made of highly porous carbon material impregnated in a liquid electrolyte and separated by a semipermeable membrane that allows the diffusion of ions but avoids the direct contact between electrodes preventing the short-circuit of the cell [6]. Taking into account that the energy stored in EDLC is proportional to the capacitance and to the square voltage ($1/2\ CV^2$), most of the strategies are focused on the capacitance increasing through the optimization of the textural properties of active materials or to the operating voltage window extension through the use of highly electrochemically stable electrolytes [7].

In this regard, activated carbons (ACs) have been the preferred choice as electrodes in high-performing EDLCs due to their large specific surface area and low cost, as well as superior physical and chemical stability. Additionally, ACs can be readily produced from worldwide abundant and easily accessible wastes [8–11]. On the other hand, the incorporation of graphene has been found to be useful for increasing the electronic conductivity of the composites by tailoring their particle morphology and textural properties [12]. Nevertheless, most of the reported works rely on the use of aqueous-based electrolytes, which considerably limits the energy density of the EDLCs due to their narrower voltage window [13–15]. Thus, the evaluation of graphene-AC composites in non-aqueous electrolytes (organic, ionic liquids) is needed to subtract its maximal potential as electrodes for advanced EDLCs [16,17]. Within this context, ionic liquids have received great interest due to their low vapor pressure, wide temperature stability range and high electrochemical stability, which allow them to operate in a stable way in a wide voltage window, thus significantly increasing the energy density of the devices [18].

Herein we have investigated the potential that industrial winery biowastes combined with graphene have as carbonaceous precursor for their use as active electrode materials for high-voltage electrical double-layer capacitors. The results point out that the presence of graphene tunes the textural properties of the final carbon and leads to an improvement in the electrochemical performances of these materials measured in both ionic liquid and conventional organic electrolytes in terms of energy and power density. However, the higher reactivity of the graphene sheets can compromise the long-term stability of the systems, especially when tested in wide operating voltage windows.

2. Materials and Methods

2.1. Materials Synthesis

Wine wastes of the "Tempranillo" variety collected from a vineyard located in Navarra (Spain) were chosen as the carbon precursor, and graphene oxide (GO) from Graphenea (4 $mg{\cdot}mL^{-1}$) was selected as the graphene source. First, wine wastes composed of skin, seeds, branches and leaves were dried at 80 °C for 4 consecutive days to subsequently crush them and convert them into waste powder. Then, 3 g of wine waste powder were mixed with 25 mL of graphene oxide and vigorously stirred for 3 h. Then, the suspension was freeze-dried for 4 days to produce the dry GO-wine waste precursor.

After that, the dried powder was pre-carbonized at 400 °C for 3 h using a heating ramp of 5 $°C{\cdot}min^{-1}$ under a dynamic Ar atmosphere in a tubular furnace. Finally, to obtain the activated carbon, the sample was ground together with KOH in a mortar using 1:4 mass ratio (C:KOH) and further heated at 800 °C for 1 h under Ar atmosphere using a heating ramp of 5 $°C{\cdot}min^{-1}$. The resulting material was washed once with a diluted solution of HCl and several times with hot deionized water and further dried to obtain the final activated carbon powder. The reduced graphene oxide-wine waste-derived activated carbon sample is hereafter denoted as rGO-WW. For the sake of comparison, an activated carbon, denoted as WW, was also prepared following the same route but in the absence of graphene oxide.

2.2. Physicochemical Characterization

Morphological characterization was performed by scanning electron microscopy (SEM) in a Quanta200 FEI (3 kV, 30 kV) microscope. The composition of the samples was char-

acterized by elemental analysis in a Flash 2000 Thermo Scientific (CHNS/O), where the samples were burned at 900 °C with an excess of oxygen. The textural properties of the composites were obtained by nitrogen adsorption/desorption isotherms that were registered at −196 °C in an ASAP 2460 from Micromeritics. The specific surface area values were calculated using the Brunauer–Emmet–Teller (BET) equation in the relative pressure range between 0.05 and 0.25, and the pore size distributions were calculated by the 2D-NLDFT model applied from the data of the adsorption branches using the SAIEUS software. Raman spectra were recorded with a Renishaw spectrometer (Nanonics multiview 2000). A laser beam with an excitation wavelength of 532 nm and 10 s exposition time was used for the spectrum acquisition.

2.3. Electrochemical Characterization

Carbon-based electrodes were processed by mixing 85% of active materials together with 10% of Super P C65 (Imerys Graphite & Carbon, Bironico, Switzerland) and 5% of polytetrafluoroethylene (PTFE) binder in the presence of ethanol. Then, the mixture was kneaded until plasticity and rolled to obtain a film with a thickness of ~100 µm. Circular-shaped electrodes of 11 mm diameter and 3.5 ± 1.5 mg were punched from the film and dried at 120 °C under vacuum overnight. The electrochemical performances of these electrodes were evaluated as symmetric EDCLs using a two-electrode Swagelok-type cell. The cells contained D-type glass fiber discs as a separator. The chosen electrolytes were 1 M tetraethylammonium tetrafluoroborate (Et_4NBF_4) in acetonitrile (ACN), and 1-ethyl-3-methylimidazolium bis(trifluoromethanesulfonyl) imide (EMINTFSI). Cyclic voltammetry (CV) and galvanostatic charge/discharge were carried out in a multichannel VMP3 generator from Biologic. The operating voltage window of each cell was selected from cyclic voltammetry measurements following the criteria reported elsewhere [19]. Applied current density (I_g) was calculated with respect to the total mass of active material (85%). Specific capacitance of the cells was obtained from the discharge branch of galvanostatic plots using Equation (1):

$$C_s = 2 \times \frac{I_g \times t_d}{\Delta V} \quad (1)$$

where t_d and ΔV are the discharge time and the operational voltage window, respectively, once the total resistance drop is subtracted. Gravimetric energy (E) and power densities (P) were calculated according to Equations (2) and (3):

$$E = \frac{1}{3.6}\left[\frac{1}{8}C_s \times \left(V_{\max}^2 - V_{\min}^2\right)\right] \quad (2)$$

$$P = \frac{E}{t_d} \quad (3)$$

where $V_{\max}$ and $V_{\min}$ are the maximum and the minimum of the cell potential, once the corresponding resistance drop is discarded.

3. Results and Discussion

As previously explained in the experimental section, an activated carbon composite comprising reduced graphene oxide/winery wastes (rGO-WW) has been synthesized as an electrode for supercapacitors. The winery wastes were firstly dispersed into a graphene oxide suspension, freeze-dried, pre-carbonized and then submitted to the activation process to increase their specific surface area and get the most appropriate balance between pore distribution, morphology and surface area [10]. On the other hand, for the sake of comparison, a pristine activated carbon derived from winery wastes (WW) was directly pre-carbonized and submitted to the activation process. SEM images registered for the materials are shown in Figure 1. It can be observed that the WW sample (Figure 1a,c) is formed by large polyhedral-shaped particles of 30–40 µm with cavities of two different sizes, 4–6 and 1.5 µm. On the other side, rGO-WW (Figure 1b,d) clearly shows the presence

of graphene sheets homogeneously distributed within the carbon particles, and the particle size is clearly reduced to 7–21 μm. The morphological differences between the two samples are immediately recognizable at higher magnification images (Figure 1c,d).

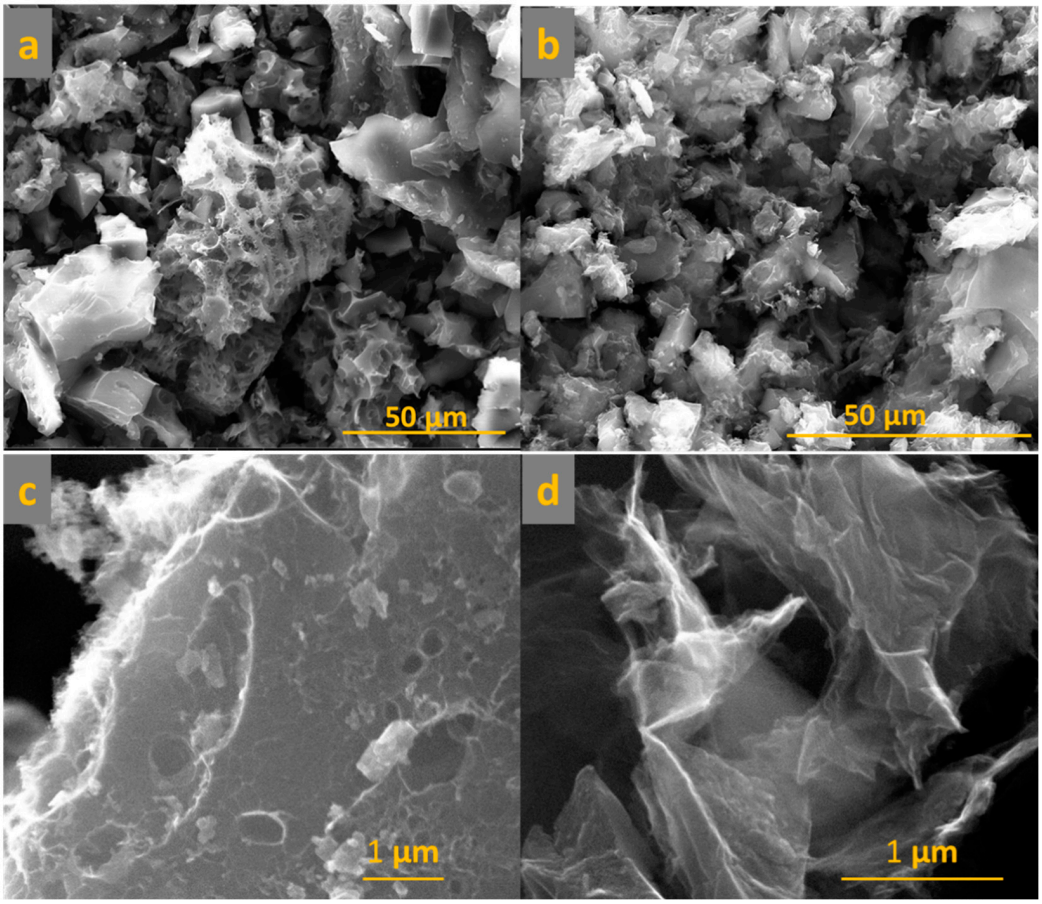

Figure 1. SEM images registered for WW (**a**,**c**) and rGO-WW (**b**,**d**) samples.

The chemical composition measured by the elemental analysis of the ACs prepared in this work is summarized in Table 1. As expected, the elemental analysis reveals that the main element in both materials is carbon (~90%). Other elements such as nitrogen, oxygen or hydrogen are present in much lower amounts. The presence of nitrogen could be, in this case, attributed to the alcoholic fermentation of grapes.

Table 1. Elemental composition of the activated carbons.

Material	% C	% O	% N	% H
WW	87.5	11.2	0.6	0.7
rGO-WW	91.2	8.3	0.2	0.2

Raman spectra were recorded to evaluate the structural differences between the two carbonaceous samples and to confirm the presence of rGO in the rGO-WW after the activation step. The Raman spectra presented in Figure 2a show the characteristics D and G bands in both WW and rGO-WW samples at ca. 1343 and ca. 1590 nm, respectively. The D and G bands are related to the presence of structural defects and graphitic domains. As expected, the addition of GO results in a smaller A_D/A_G ratio, pointing out a lower disorder degree. Additionally, the Raman spectrum of rGO-WW shows a band at ca. 2680 nm corresponding with the 2D band. This band is related to the 2D morphology of the rGO and confirms the proper conservation of the rGO sheets after the activation step.

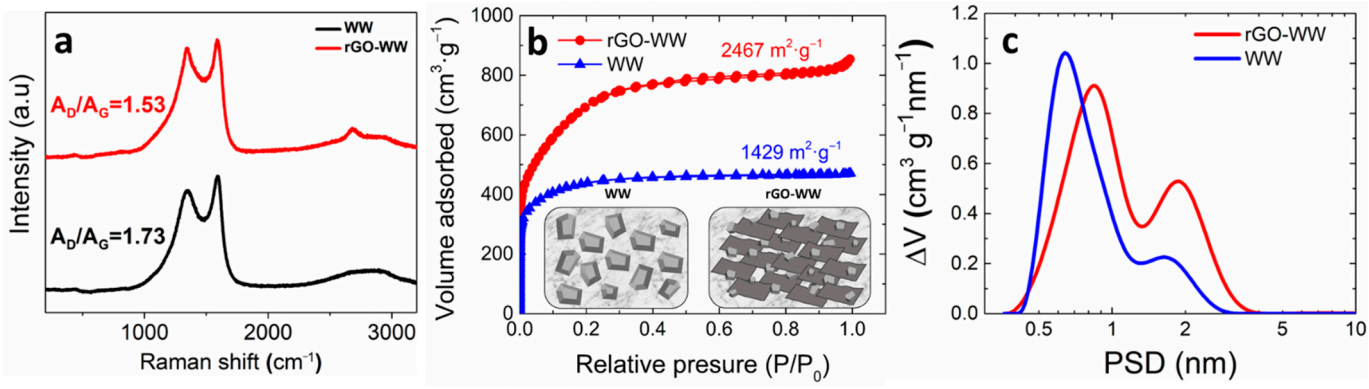

Figure 2. Raman spectra (**a**), nitrogen adsorption/desorption isotherms (**b**) and pore size distributions (**c**) measured for indicated samples.

Nitrogen adsorption/desorption isotherms were registered in order to assess the textural properties of the materials. Figure 2b,c include the isotherms registered for these samples and the pore size distributions associated with each of them. Both materials show similar adsorption profiles matching with type-I isotherms according to the IUPAC classification, which corresponds to porous samples with pores within the microporous range (<2 nm) [20]. The BET-specific surface area calculated for rGO-WW and WW gives values of 2467 and 1429 $m^2 \cdot g^{-1}$, respectively. A schematic representation of the particle shape and size of the samples has been included in Figure 2b. The 2D characteristic of the rGO sheets and the effect of the carbon particles acting as spacers are responsible for the specific surface area increment, also modifying the pore size of rGO-WW. Regarding the pore size distribution, the sample containing graphene oxide (rGO-WW) contains medium-size micropores centered at 0.9 nm and large-sized micropores of around 2 nm, while the sample without graphene oxide (WW) contains small-size pores of 0.7 nm and a few larger ones at ca. 1.6 nm.

According to these results, it seems that the presence of the graphene sheets within the rGO-WW sample helps to maximize the activation process giving rise to carbons with much larger specific surface areas and wider pores compared to the graphene-free sample (WW). It is worth remarking that the specific surface area achieved for the rGO-WW composite surpasses most of the carbons derived from winery wastes in the reported literature [13–15,21–25].

These homemade carbonaceous materials were evaluated as active materials in a two-electrode symmetric configuration using the conventional organic electrolyte 1 M Et_4NBF_4/ACN and the bare ionic liquid EMINTFSI. Figure 3 shows the CV curves registered for the supercapacitor cells at different sweep rates in the previously determined operating voltage window. From these CV curves, a much better electrochemical stability can be assessed for those systems measured in ionic liquid, which enables the expansion of the operating voltage window compared to those measured in the organic electrolyte. Moreover, the graphene-free sample (WW) seems to be more stable electrochemically than the composite (rGO-WW). Specifically, operating voltage windows of 2.9 and 3.1 V were determined for the WW sample (Figure 3a,c) and 2.7 and 2.9 V for the composite rGO-WW (Figure 3b,d) in the electrolytes 1 M Et_4NBF_4/ACN and EMINTFSI, respectively. Both materials show typical rectangular-shaped profiles, which are characteristic of capacitive-type charge storage mechanisms [26]. The graphene-containing sample rGO-WW outperforms the pristine WW whenever the electrolyte is tested in terms of specific capacitance and capacitance retention. This can be ascribed to the enhancement of the specific surface area and the pore widening upon graphene addition to the winery wastes, as previously explained.

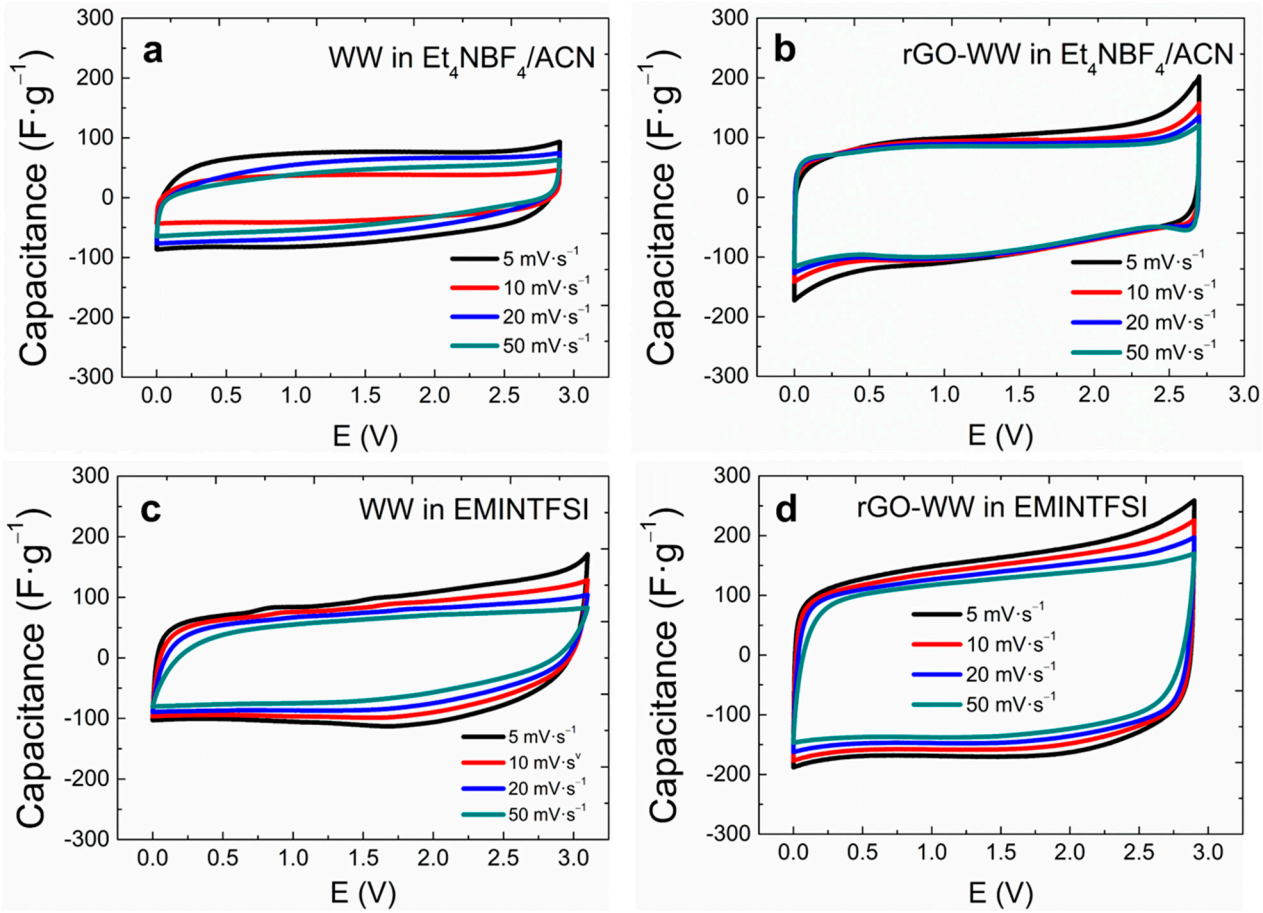

Figure 3. Cyclic voltammetry curves registered for supercapacitors assembled using WW in 1 M Et_4NBF_4 (**a**), and EMINTFSI (**c**); and corresponding measurements for rGO-WW (**b**,**d**).

Galvanostatic charge/discharge curves at different current densities registered for these samples at 0.5 and 5 $A \cdot g^{-1}$ are depicted in Figure 4. It can be observed that all samples show linear voltage increase/decrease during charge and discharge with the typical triangular shape of capacitive-type charge storage mechanisms. At the low current density of 0.5 $A \cdot g^{-1}$, both ACs show very small ohmic drop (Figure 4a,c), which are progressively enlarged as the current rate is increased to 5 $A \cdot g^{-1}$ (Figure 4b,d). It is worth highlighting that this behavior is more pronounced for the EDLCs measured in the ionic liquid (EMINTFSI) due to its lower ionic conductivity and its higher viscosity compared to the organic electrolyte (Et_4NBF_4) (see Table 2). The sample without graphene oxide exhibits a larger ohmic drop compared to the graphene-containing one, which could be associated to its lower electronic conductivity.

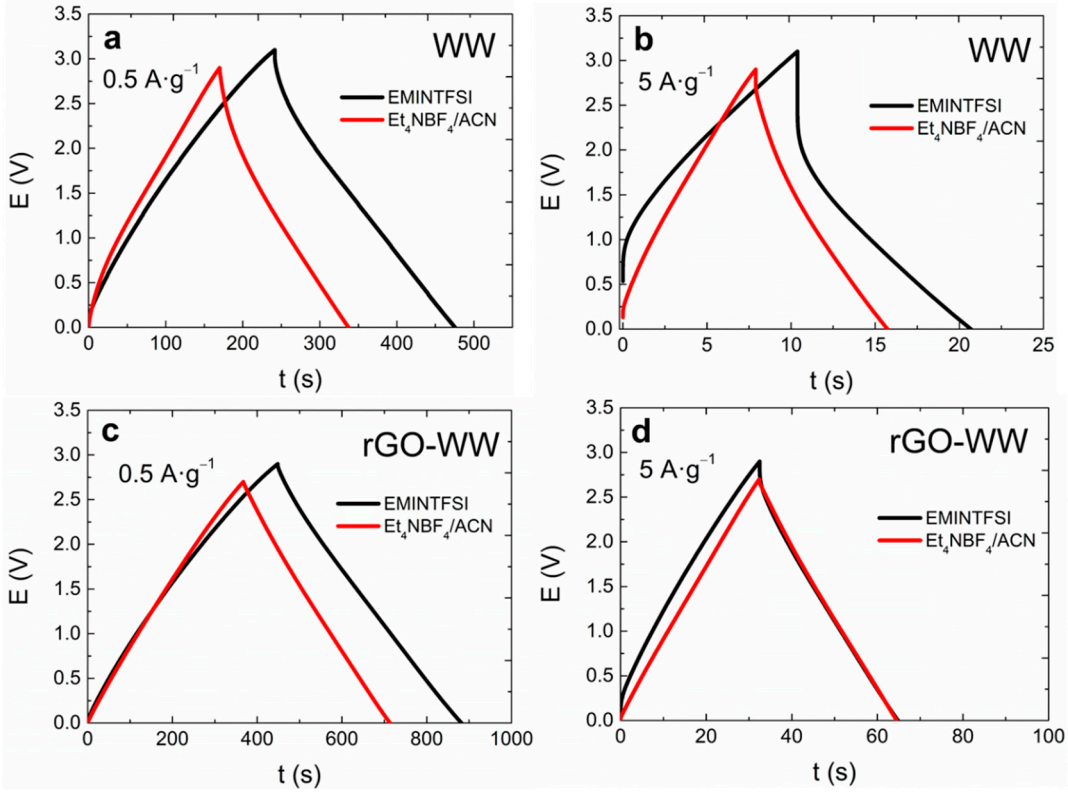

Figure 4. Galvanostatic charge-discharge curves registered in both electrolytes for WW sample at 0.5 (**a**) and 5 $A \cdot g^{-1}$ (**b**); and corresponding measurements for rGO-WW (**c**,**d**).

Table 2. Physical properties of the selected electrolytes.

Electrolyte	Viscosity (mPa·s)	Conductivity ($mS \cdot cm^{-1}$)	Cation Size (nm)	Anion Size (nm)	Ref.
1 M Et_4NBF_4/ACN	0.57	63	0.69	0.46	[27]
EMINTFSI	35.55	9	0.76	0.79	[28]

The evolution of the specific capacitance values at different current rates for the two electrolytes, calculated from the discharge branch of galvanostatic curves, are shown in Figure 5a. In good agreement with the CV results, the specific capacitance of the composite rGO-WW is larger than that of the pristine WW regardless of the electrolyte used. In fact, at low current densities, rGO-WW doubles the specific capacitance of WW either in the IL (160 $F \cdot g^{-1}$ vs. 79 $F \cdot g^{-2}$) or in the organic electrolyte (130 $F \cdot g^{-1}$ vs. 65 $F \cdot g^{-1}$). It is also worth highlighting that at low current densities, the specific capacitance measured for both samples is significantly larger in the ionic liquid compared to the organic electrolyte. This has been previously explained by the improved ion confinement in the pores of EMINTFSI due to the geometry of the ions [29]. In contrast, samples measured in the organic electrolyte exhibit better capacitance retention due to its lower viscosity and higher ionic conductivity (Table 2) (Figure 5b). Furthermore, at high current densities, the diffusion to the pores is not favored, and this takes special relevancy when the electrolytes are formed by large size ions, as in the case of ionic liquids (Table 2). Nevertheless, regardless of the electrolyte used, the graphene-containing sample exhibits much higher capacitance retention than the pristine (86% for rGO-WW vs. 72% for WW in 1 M Et_4NBF_4/ACN and 40% for rGO-WW vs. 11% for WW in EMINTFSI) (Figure 5b).

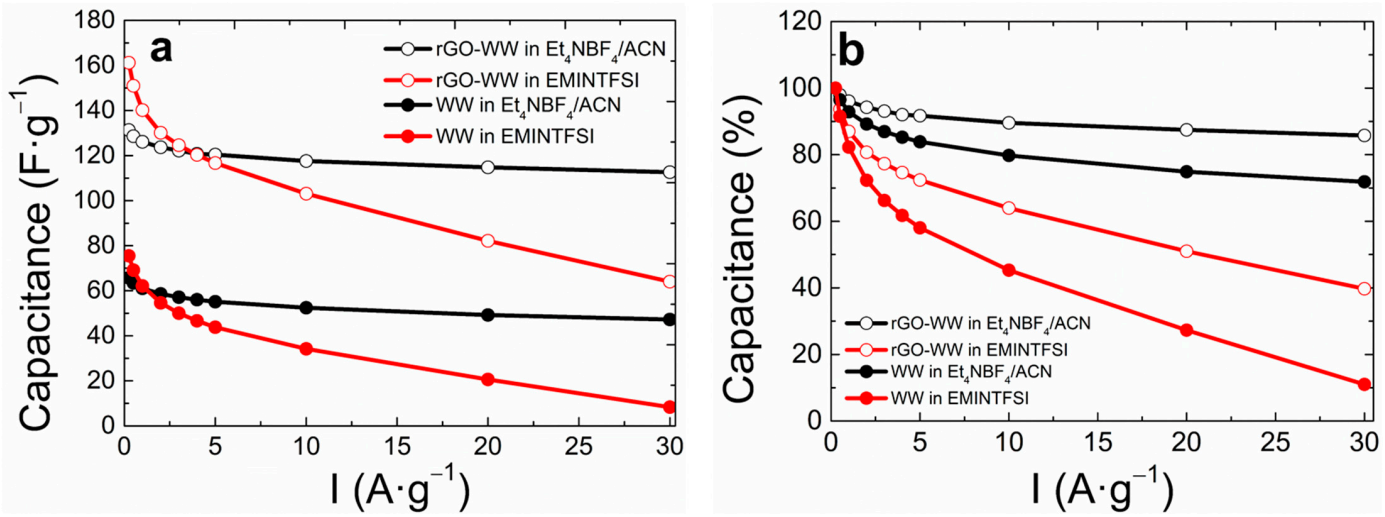

Figure 5. Capacitance evolution vs. current density (**a**) and capacitance retention (**b**) of noted samples.

The energy-to-power density plot for these home-designed symmetric cells is shown in Figure 6. Ragone plots confirm the larger energy density values and better power performance of graphene-wine waste (rGO-WW) electrode-based systems due to its larger specific capacitance and improved electronic conductivity. The systems measured using the ionic liquid EMINTFSI as electrolyte show maximized energy density values at low power densities due to the wider operating voltage window (46 W·h·kg^{-1} at 180 W·kg^{-1} for rGO-WW and 24 W·h·kg^{-1} at 191 W·kg^{-1} for WW) compared to the conventional organic electrolyte 1 M Et_4NBF_4/ACN (33.1 W·h·kg^{-1} at 160 W·kg^{-1} for rGO-WW and 19.1 W·h·kg^{-1} at 181 W·kg^{-1} for WW). However, EDLCs measured in the IL show a much more prominent decay at high power densities. In fact, 82% and 65% of the energy is still delivered for the supercapacitors rGO-WW, and WW assembled in the organic electrolyte at the maximum power rate, while only 38% and 7% are delivered for those using the pure ionic liquid.

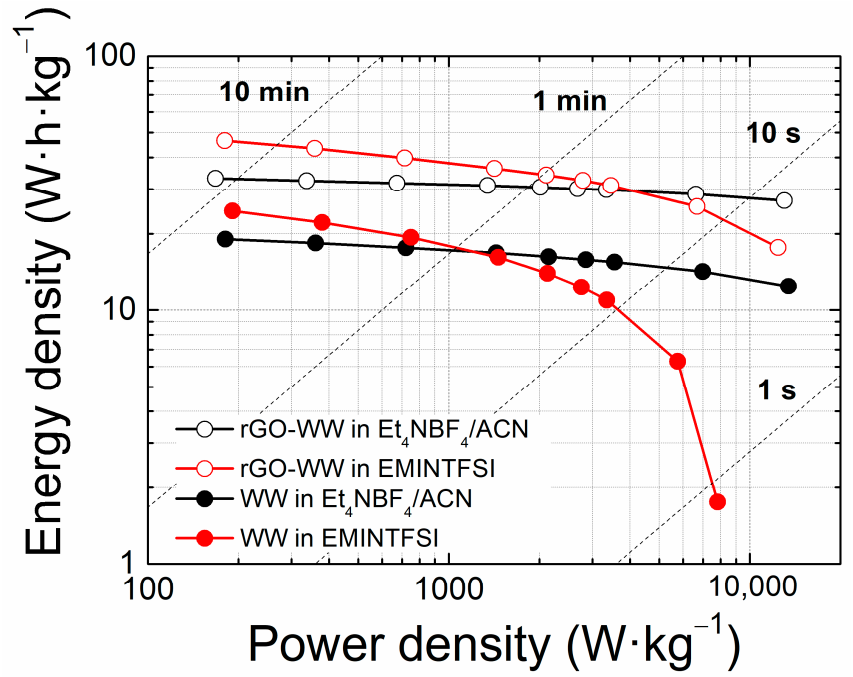

Figure 6. Ragone plot of indicated samples in both electrolytes.

These results are in line with most representative biowaste-derived carbons reported in the literature using organic and ionic liquid electrolytes. It is true that the specific capacitance of our reduced graphene oxide/winery waste-derived carbon surpasses most of these materials, and the energy delivered is similar or even lower [10,30–33]. This could be related to the higher reactivity of the graphene sheets, especially in the ionic liquid, which could represent a handicap narrowing the operational voltage as well as compromising the cycling stability. Taking this into account and the exceptional electrochemical performance of both AC in the organic electrolyte, the stability of these EDLC systems was evaluated by monitoring the specific capacitance value from galvanostatic charge/discharge measurements at 10 $A \cdot g^{-1}$ at regular intervals (Figure 7).

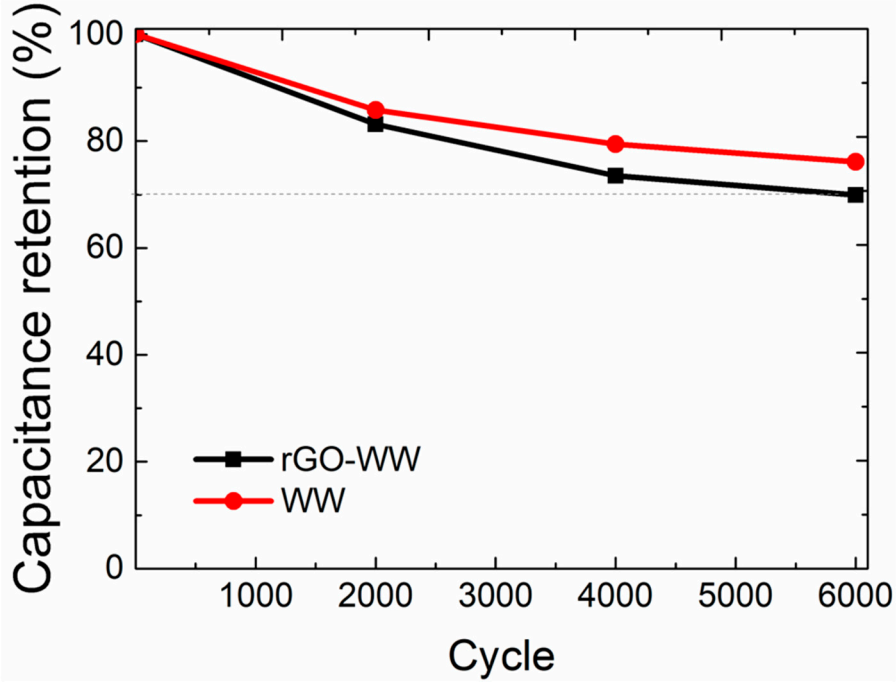

Figure 7. Capacitance evolution along cycles of indicated samples measured at 10 $A \cdot g^{-1}$ in the organic electrolyte.

The cyclability measurement shows that WW still retains 78% of the initial capacitance after 6000 cycles compared to the 70% of capacitance retention measured for the rGO-WW. Once again, this can be ascribed to the higher reactivity of samples containing graphene oxide that may arise as a consequence of their larger concentration of oxygen groups of the graphene oxide that react with the electrolyte and promote its degradation.

4. Conclusions

Winery wastes were demonstrated as promising raw material for its revalorization as a porous carbon. The optimization of different parameters, such as particle size, electronic conductivity and specific surface areas plays a significant role and have a huge impact on the final electrochemical performance of these materials as electrodes for symmetric supercapacitors.

The results show that the reduced graphene oxide notably improved the electrochemical properties of these devices. The most favorable results in terms of energy, power density and stability are obtained for supercapacitors operating with an organic electrolyte (~27 $W \cdot h \cdot kg^{-1}$ at 13,026 $W \cdot kg^{-1}$). The choice of ionic liquid as the electrolyte can also provide some important advantages under some specific operating conditions, specifically at low power densities.

In summary, the reutilization of agricultural waste as a precursor of active material for electrodes in double-layer supercapacitors is a sustainable, innovative solution. Furthermore, the presence of reduced graphene oxide improved the energy and power density,

but due to their higher reactivity, the stability can be compromised in the long term. These supercapacitors still retain more than 70% of their initial capacitance after more than 6000 charge-discharge cycles.

Author Contributions: Conceptualization, D.C.; Funding acquisition, D.C.; Investigation, V.U.-T., G.M.-F., J.L.G.-U. and M.G.-M.; Methodology, V.U.-T., G.M.-F., J.L.G.-U. and M.G.-M.; Supervision, G.M.-F. and D.C.; Validation, J.L.G.-U. and M.G.-M.; Writing—original draft, G.M.-F.; Writing—review and editing, V.U.-T., J.L.G.-U., M.G.-M. and D.C. All authors have read and agreed to the published version of the manuscript.

Funding: This research was funded by the European Union through the project Graphene Flagship, Core 3, Grant number 881603; by the Spanish ministry of Science and Innovation through the project MICINN/FEDER (RTI2018-096199-B-I00); and by the Spanish Ministry of Education, Science and Universities through the FPU grant (16/03498).

Institutional Review Board Statement: Not applicable.

Data Availability Statement: Data are available upon request to the authors.

Acknowledgments: The authors thank the European Union (Graphene Flagship, Core 3, Grant number 881603) and the Spanish Ministry of Science and Innovation (MICINN/FEDER) (RTI2018-096199-B-I00) for the financial support of this work. J.L.G.-U. is very thankful to the Spanish Ministry of Education, Science and Universities (MICINN) for the FPU grant (16/03498). We also want to acknowledge the company GRAPHENEA for supplying the graphene oxide used in this work.

Conflicts of Interest: The authors declare no conflict of interest. The funders had no role in the design of the study; in the collection, analyses, or interpretation of data; in the writing of the manuscript, or in the decision to publish the results.

References

1. Koohi-Fayegh, S.; Rosen, M.A. A Review of Energy Storage Types, Applications and Recent Developments. *J. Energy Storage* **2020**, *27*, 101047. [CrossRef]
2. Hannan, M.A.; Hoque, M.M.; Mohamed, A.; Ayob, A. Review of Energy Storage Systems for Electric Vehicle Applications: Issues and Challenges. *Renew. Sustain. Energy Rev.* **2017**, *69*, 771–789. [CrossRef]
3. Li, M.; Lu, J.; Chen, Z.; Amine, K. 30 Years of Lithium-Ion Batteries. *Adv. Mater.* **2018**, *30*, 1800561. [CrossRef] [PubMed]
4. Poonam; Sharma, K.; Arora, A.; Tripathi, S.K. Review of Supercapacitors: Materials and Devices. *J. Energy Storage* **2019**, *21*, 801–825. [CrossRef]
5. Simon, P.; Gogotsi, Y.; Dunn, B. Where Do Batteries End and Supercapacitors Begin? *Science* **2014**, *343*, 1210–1211. [CrossRef]
6. Zhao, J.; Burke, A.F. Review on Supercapacitors: Technologies and Performance Evaluation. *J. Energy Chem.* **2021**, *59*, 276–291. [CrossRef]
7. González, A.; Goikolea, E.; Barrena, J.A.; Mysyk, R. Review on Supercapacitors: Technologies and Materials. *Renew. Sustain. Energy Rev.* **2016**, *58*, 1189–1206. [CrossRef]
8. Díez, N.; Botas, C.; Mysyk, R.; Goikolea, E.; Rojo, T.; Carriazo, D. Highly Packed Graphene–CNT Films as Electrodes for Aqueous Supercapacitors with High Volumetric Performance. *J. Mater. Chem. A* **2018**, *6*, 3667–3673. [CrossRef]
9. Moreno-Fernández, G.; Gómez-Urbano, J.L.; Enterría, M.; Rojo, T.; Carriazo, D. Flat-Shaped Carbon–Graphene Microcomposites as Electrodes for High Energy Supercapacitors. *J. Mater. Chem. A* **2019**, *7*, 14646–14655. [CrossRef]
10. Gómez-Urbano, J.L.; Moreno-Fernández, G.; Granados-Moreno, M.; Rojo, T.; Carriazo, D. Nanostructured Carbon Composites from Cigarette Filter Wastes and Graphene Oxide Suitable as Electrodes for 3.4 V Supercapacitors. *Batter. Supercaps* **2021**, *4*, 1749–1756. [CrossRef]
11. Gómez-Urbano, J.L.; Moreno-Fernández, G.; Arnaiz, M.; Ajuria, J.; Rojo, T.; Carriazo, D. Graphene-Coffee Waste Derived Carbon Composites as Electrodes for Optimized Lithium Ion Capacitors. *Carbon* **2020**, *162*, 273–282. [CrossRef]
12. Cheng, F.; Yang, X.; Zhang, S.; Lu, W. Boosting the Supercapacitor Performances of Activated Carbon with Carbon Nanomaterials. *J. Power Sources* **2020**, *450*, 227678. [CrossRef]
13. Guardia, L.; Suárez, L.; Querejeta, N.; Pevida, C.; Centeno, T.A. Winery Wastes as Precursors of Sustainable Porous Carbons for Environmental Applications. *J. Clean. Prod.* **2018**, *193*, 614–624. [CrossRef]
14. Suárez, L.; Centeno, T.A. Unravelling the Volumetric Performance of Activated Carbons from Biomass Wastes in Supercapacitors. *J. Power Sources* **2020**, *448*, 227413. [CrossRef]
15. Jiménez-Cordero, D.; Heras, F.; Gilarranz, M.A.; Raymundo-Piñero, E. Grape Seed Carbons for Studying the Influence of Texture on Supercapacitor Behaviour in Aqueous Electrolytes. *Carbon* **2014**, *71*, 127–138. [CrossRef]
16. Díez, N.; Mysyk, R.; Zhang, W.; Goikolea, E.; Carriazo, D. One-Pot Synthesis of Highly Activated Carbons from Melamine and Terephthalaldehyde as Electrodes for High Energy Aqueous Supercapacitors. *J. Mater. Chem. A* **2017**, *5*, 14619–14629. [CrossRef]

17. Moreno-Fernández, G.; Boulanger, N.; Nordenström, A.; Iakunkov, A.; Talyzin, A.; Carriazo, D.; Mysyk, R. Ball-Milling-Enhanced Capacitive Charge Storage of Activated Graphene in Aqueous, Organic and Ionic Liquid Electrolytes. *Electrochim. Acta* **2021**, *370*, 137738. [CrossRef]
18. Brandt, A.; Pohlmann, S.; Varzi, A.; Balducci, A.; Passerini, S. Ionic Liquids in Supercapacitors. *MRS Bull.* **2013**, *38*, 554–559. [CrossRef]
19. Bahdanchyk, M.; Hashempour, M.; Vicenzo, A. Evaluation of the Operating Potential Window of Electrochemical Capacitors. *Electrochim. Acta* **2020**, *332*, 135503. [CrossRef]
20. Thommes, M.; Kaneko, K.; Neimark, A.V.; Olivier, J.P.; Rodriguez-Reinoso, F.; Rouquerol, J.; Sing, K.S.W. Physisorption of Gases, with Special Reference to the Evaluation of Surface Area and Pore Size Distribution (IUPAC Technical Report). *Pure Appl. Chem.* **2015**, *87*, 1051–1069. [CrossRef]
21. Guardia, L.; Suárez, L.; Querejeta, N.; Vretenár, V.; Kotrusz, P.; Skákalová, V.; Centeno, T.A. Biomass Waste-Carbon/Reduced Graphene Oxide Composite Electrodes for Enhanced Supercapacitors. *Electrochim. Acta* **2019**, *298*, 910–917. [CrossRef]
22. Zuo, X.; Chang, K.; Zhao, J.; Xie, Z.; Tang, H.; Li, B.; Chang, Z. Bubble-Template-Assisted Synthesis of Hollow Fullerene-like MoS_2 Nanocages as a Lithium Ion Battery Anode Material. *J. Mater. Chem. A* **2016**, *4*, 51–58. [CrossRef]
23. Hoffmann, V.; Jung, D.; Zimmermann, J.; Rodriguez Correa, C.; Elleuch, A.; Halouani, K.; Kruse, A. Conductive Carbon Materials from the Hydrothermal Carbonization of Vineyard Residues for the Application in Electrochemical Double-Layer Capacitors (EDLCs) and Direct Carbon Fuel Cells (DCFCs). *Materials* **2019**, *12*, 1703. [CrossRef] [PubMed]
24. Ramanathan, S.; Moorthy, S.; Ramasundaram, S.; Rajan, H.K.; Vishwanath, S.; Selvinsimpson, S.; Durairaj, A.; Kim, B.; Vasanthkumar, S. Grape Seed Extract Assisted Synthesis of Dual-Functional Anatase TiO_2 Decorated Reduced Graphene Oxide Composite for Supercapacitor Electrode Material and Visible Light Photocatalytic Degradation of Bromophenol Blue Dye. *ACS Omega* **2021**, *6*, 14734–14747. [CrossRef] [PubMed]
25. Zhang, J.; Chen, H.; Bai, J.; Xu, M.; Luo, C.; Yang, L.; Bai, L.; Wei, D.; Wang, W.; Yang, H. N-Doped Hierarchically Porous Carbon Derived from Grape Marcs for High-Performance Supercapacitors. *J. Alloys Compd.* **2021**, *854*, 157207. [CrossRef]
26. Babu, B.; Simon, P.; Balducci, A. Fast Charging Materials for High Power Applications. *Adv. Energy Mater.* **2020**, *10*, 2001128. [CrossRef]
27. Pohlmann, S.; Kühnel, R.-S.; Centeno, T.A.; Balducci, A. The Influence of Anion-Cation Combinations on the Physicochemical Properties of Advanced Electrolytes for Supercapacitors and the Capacitance of Activated Carbons. *ChemElectroChem* **2014**, *1*, 1301–1311. [CrossRef]
28. Singh, R.; Rajput, N.N.; He, X.; Monk, J.; Hung, F.R. Molecular Dynamics Simulations of the Ionic Liquid [EMIM+][TFMSI−] Confined inside Rutile (110) Slit Nanopores. *Phys. Chem. Chem. Phys.* **2013**, *15*, 16090. [CrossRef]
29. Merlet, C.; Péan, C.; Rotenberg, B.; Madden, P.A.; Daffos, B.; Taberna, P.-L.; Simon, P.; Salanne, M. Highly Confined Ions Store Charge More Efficiently in Supercapacitors. *Nat. Commun.* **2013**, *4*, 2701. [CrossRef]
30. Momodu, D.; Sylla, N.F.; Mutuma, B.; Bello, A.; Masikhwa, T.; Lindberg, S.; Matic, A.; Manyala, N. Stable Ionic-Liquid-Based Symmetric Supercapacitors from Capsicum Seed-Porous Carbons. *J. Electroanal. Chem.* **2019**, *838*, 119–128. [CrossRef]
31. Cui, Y.; Wang, H.; Mao, N.; Yu, W.; Shi, J.; Huang, M.; Liu, W.; Chen, S.; Wang, X. Tuning the Morphology and Structure of Nanocarbons with Activating Agents for Ultrafast Ionic Liquid-Based Supercapacitors. *J. Power Sources* **2017**, *361*, 182–194. [CrossRef]
32. Tian, W.; Gao, Q.; Tan, Y.; Yang, K.; Zhu, L.; Yang, C.; Zhang, H. Bio-Inspired Beehive-like Hierarchical Nanoporous Carbon Derived from Bamboo-Based Industrial by-Product as a High Performance Supercapacitor Electrode Material. *J. Mater. Chem. A* **2015**, *3*, 5656–5664. [CrossRef]
33. Wang, H.; Li, Z.; Tak, J.K.; Holt, C.M.B.; Tan, X.; Xu, Z.; Amirkhiz, B.S.; Harfield, D.; Anyia, A.; Stephenson, T.; et al. Supercapacitors Based on Carbons with Tuned Porosity Derived from Paper Pulp Mill Sludge Biowaste. *Carbon* **2013**, *57*, 317–328. [CrossRef]